Imaging Superficial Tissues With Polarized Light

Steven L. Jacques, PhD,[1,2,3]* Jessica R. Roman, MS,[1,2] and Ken Lee, MD[3]

[1]Oregon Medical Laser Center, Providence St. Vincent Medical Center, Portland, Oregon 97225
[2]Electrical and Computer Engineering, Oregon Graduate Institute, Portland, Oregon 97006
[3]Oregon Health Sciences University, Portland, Oregon 97201

Objective: **Polarized light can be used to obtain images of superficial tissue layers such as skin, and some example images are presented. This study presents a study of the transition of linearly polarized light into randomly polarized light during light propagation through tissues.**
Study Design/Materials and Methods: **The transition of polarization was studied in polystyrene microsphere solutions, in chicken muscle (breast) and liver, and in porcine muscle and skin. The transition is discussed in terms of a diffusion process characterized by an angular diffusivity (radians^2/mean free path) for the change in angular orientation of linearly polarized light per unit optical path traveled by the light.**
Results: **Microsphere diffusivity increased from 0.031 to 0.800 for diameters decreasing from 6.04 μm to 0.306 μm, respectively. Tissue diffusivity varied from a very low value (0.0004) for chicken liver to an intermediate value (0.055) for chicken and porcine muscle to a very high value (0.78) for pig skin.**
Conclusion: **The results are consistent with the hypothesis that birefringent tissues randomize linearly polarized light more rapidly than nonbirefringent tissues. The results suggest that polarized light imaging of skin yields images based only on photons backscattered from the superficial epidermal and initial papillary dermis because the birefringent dermal collagen rapidly randomizes polarized light. This anatomic region of the skin is where cancer commonly arises. Lasers Surg. Med. 26:119–129, 2000.** © 2000 Wiley-Liss, Inc.

Key words: imaging; polarized light; tissue optical properties; muscle; liver; polystyrene microspheres

INTRODUCTION

Cancer often arises in the superficial epithelial layers of a tissue. Skin cancer, for example, usually arises in the epidermis. The doctor's eye has difficulty seeing superficial tissue layers when most of the backscattered light originates from the deeper tissue layers. An imaging system based on photons that backscatter from superficial tissue layers can yield images whose contrast is concentrated in the region of interest.

We are currently developing a polarized light camera for optical imaging of superficial tissues by using reflected polarized light [1]. The camera creates an image whose contrast is concentrated in the superficial layers of tissues where cancer often arises. Such images are here called polarization images. Polarization images allow the doctor to see the margins of cancers visually rather than requiring histologic evaluation such as in Mohs surgery of skin cancers. The images do not replace histologic evaluation but would help the

Mohs surgeon estimate the cancer margins so as to minimize the number of histologic evaluations required and the net time of the procedure. The following sections of this introduction will briefly review some of the previous work on the use of polarized light in medicine then briefly describe the polarized light camera system, which is the motivation for the experiments of this study.

This study attempts to more fully understand the basis for polarization images. The study reports experimental studies of how the orientation of linearly polarized light is randomized by scattering during propagation through biological tissues and through aqueous solutions of polystyrene spheres. The loss of orientation is discussed in terms of an angular diffusivity for the angle of orientation of linearly polarized light. The experiments were conducted in transmission mode where photons propagated through a cuvette containing tissue or microsphere solutions and were detected on the backside of the sample. The results enable specification of a hypothesis for the mechanism and depth of imaging for polarization images of skin by using reflected light.

Previous Literature

The use of polarized light measurements is well developed [e.g., Refs. 2–4]. One can purchase commercial equipment that will conduct a variety of polarization measurements. A large amount of work on polarization backscatter has characterized atmospheric optics and earth imaging from satellites. In medicine and biology, the use of polarized light to characterize cells and tissues has a long history, beginning with studies of cell suspensions and more recently with studies of turbid tissue phantoms and in vivo tissues. Bickel et al. [5] introduced polarized light as a method for studying light scattering by *Bacillus subtilis*. Anderson [6] summarized the clinical dermatology experience with polarized light in which the doctor can choose to accent (or reject) surface glare by viewing the skin through polarizing filters oriented parallel (or perpendicular) to the polarization of the illumination light. This phenomenon is akin to the common Polaroid sunglasses that reject the horizontally polarized glare off road surfaces by viewing through vertically polarized filters. Schmitt et al. [7] reported how linearly and circularly polarized light are transmitted through turbid media and outlined the use of the scattering matrix and Müller matrix to discuss such transport. Dogariu and Asakura [8] measured the azimuthal pattern of polarized

backscattered light to specify average photon pathlengths in turbid media. Jacques et al. used video reflectometry to study the point spread function for polarized light in aqueous solutions of polystyrene spheres [9] and in skin [10]. They observed that the point spread function for reflected polarized light from skin was quite localized, suggesting that polarization images would not suffer from excessive blurring. Hielscher et al. [11] made important observations on how the point spread function for reflected polarized light could specify the optical properties and scattering particle size of a medium. They reported unique scattering patterns from yeast and fibroblast cell suspensions demonstrating the potential for characterizing cells. Demos and Alfano [12] reported time-resolved polarization backscatter measurements and implemented a CCD camera to create images based on backscattered polarized light. Hielscher et al. [13] implemented the full Müller matrix description of linearly and circularly polarized light transport and applied this to video images of point spread functions in both phantoms and solutions of cells, reporting patterns of polarized backscatter that discriminated cancerous from noncancerous cells in suspension. Jacques and Lee [1] gave a preliminary report on polarization images of skin taken in a clinical setting, illustrating the feasibility of polarization images to detect skin pathology and to identify cancer margins to guide surgical excision. Cameron et al. [14] implemented the Müller matrix description of polarized light scattering in a Monte Carlo simulation that recreated the familiar cross pattern observed in reflectance images from polystyrene sphere suspensions. Mourant et al. [15] reported the wavelength dependence of polarized light scattering in normal versus cancer cells in culture.

Similar experiments to those in this study were reported by Jarry et al. [16] They studied HeNe laser (633 nm) polarized light transmission through polystyrene microsphere solutions and liver tissue. Their experimental data will be analyzed by using the analysis method of this study and compared with the experimental results of this report.

Polarized Light Camera

Figure 1 shows a schematic for the polarization imaging camera. White light is chosen for illumination to avoid the effect of laser speckle. The white light is linearly polarized by a linearly polarizing filter (Oriel) oriented parallel to the plane established by the source-skin-camera tri-
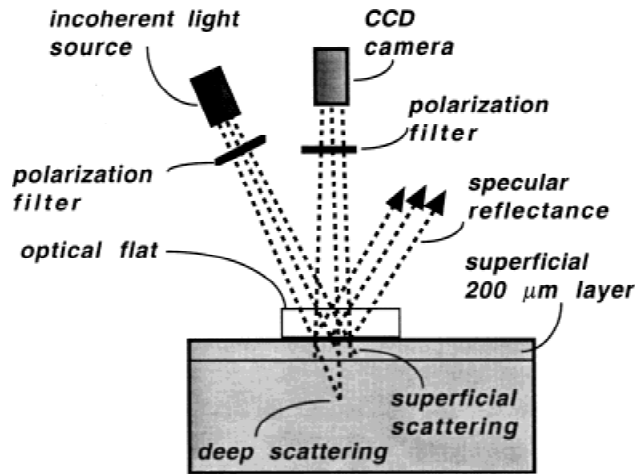
Fig. 1. Basic polarized light camera system. The second polarizer in front of the camera is oriented to select light either parallel to or light perpendicular to the incident to yield two images, I_{par} and I_{per}. The two images are combined by using equation 1 to yield a polarization image (see Fig. 2).

angle. A glass optical flat is pressed against the skin with a drop of water for index matching to enforce a flat skin surface and redirect the glare off the skin surface due to specular reflectance. Consequently, the glare at the air/glass surface and at the glass/skin surface is directed at an oblique angle away from the camera. The glare constitutes about 4% of the incident light. Only light that enters the skin and backscatters toward the surface will be collected by the camera.

As the polarized light enters the skin, back reflectance of light from the initial skin layers is observed by the camera. This initial back reflectance to some degree retains the linear polarization of the incident light, and constitutes roughly about 3% of the incident light. The remaining 93% of the incident light penetrates deep into the reticular dermis, and the orientation of polarization becomes randomized by multiple scattering events. Eventually, about half of this deeply penetrating light is lost to absorption, but half of the light is backscattered to the surface, escapes the skin, and is viewed by the camera. Hence, about 45% of the incident light escapes as randomly polarized light.

The camera is used to acquire two images. A linear polarization filter in front of the camera can be rotated to accept light parallel to the incident light or perpendicular to the incident light. The first image collects light with the polarizer oriented to accept light parallel to the incident light, and the image is called I_{par}. The second image collects light with the polarizer oriented to

accept light perpendicular to the incident light, and the image is called I_{per}. The two images are used to create a third image called the polarization image, I_{pol}:

$$I_{pol} = \frac{I_{par} - I_{per}}{I_{pol} + I_{per}}. \qquad (1)$$

The numerator takes the difference between the two acquired images. Because the randomly polarized light contributes equally to both these images, random contribution is eliminated by the subtraction. The denominator takes the sum of the two acquired images, which is equivalent to a normal white light image. Taking the ratio of the difference over the sum has an additional advantage. Epidermal melanin acts as an absorption filter and contributes a common attenuation factor to both I_{par} and I_{per}. The ratio cancels out this common attenuation factor. Therefore, essentially superficial melanin is removed from the image.

The oriented polarized light components of I_{par} and I_{per} are roughly 3% and 0% of the incident light. The randomly polarized components of I_{par} and I_{per} are roughly 22.5% and 22.5% of the incident light. Hence, the pixel values of a typical polarization image, I_{pol}, should be approximately $(25.5\% - 22.5\%)/(22.5\% + 22.5\%) = 0.067$, which is seen experimentally. The above estimate has assumed that the camera collection equally samples the backscattered I_{par} and the randomized diffusely backscattered light ($I_{par} + I_{per}$). If this assumption is not correct, then the estimate that I_{par} constitutes 3% of incident light needs adjustment. The experimental observation is that I_{pol} values have pixel values of 0.04–0.07.

Figure 2 shows normal white light and polarization images for two cases, a freckle and a benign pigmented nevus. A half dozen freckles and pigmented nevi were photographed, and they all presented the behavior shown in Figure 2. The melanin of the freckle is apparent in the normal white light image, but the melanin has been eliminated by subtraction in the polarization image. The melanin of the benign nevus is very strong in the normal white light image, but has been removed in the polarization image. Yet, there is significant structure apparent in the polarization image of the nevus. The origin of such structure is still being studied. Possibly the polarized light is backscattered off the melanosomes to contribute to I_{pol}. The reflectance of polarized light from melanosomes depends on the refractive
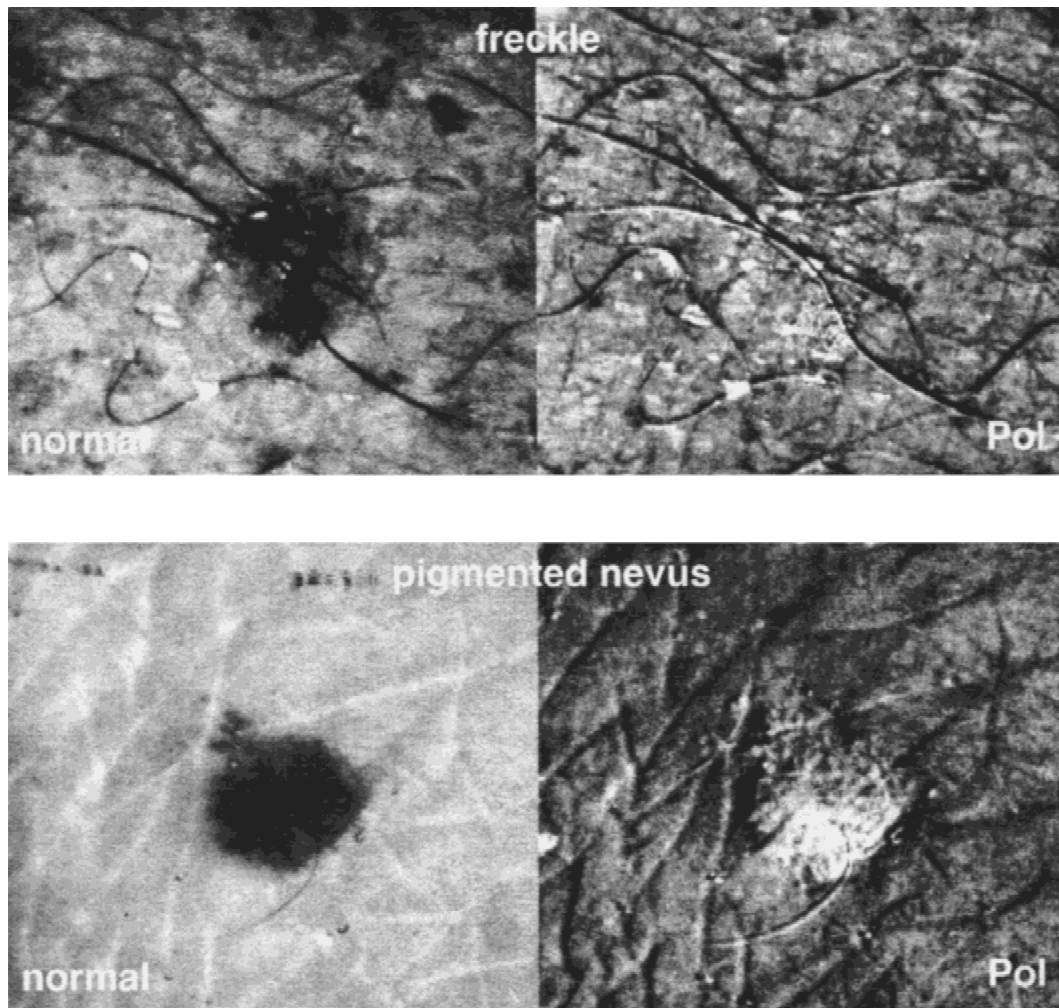
Fig. 2. Normal white light and polarization images of freckle and benign nevus. **Top:** the polarization image has removed the melanin of the freckle. **Bottom:** the polarization image reveals the structure of a benign pigmented nevus. Reprinted with permission from SPIE [1].

index of the melanosome, which is determined by both the absorption and scattering properties of the melanosome. However, the melanosomes of the freckle did not seem to contribute to I_{pol}. Possibly the melanin of the nevus is subsurface and no longer acts as a simple surface filter; hence, the melanin is not completely eliminated by taking the ratio in equation 1. Work continues on interpretation of polarization images.

MATERIALS AND METHODS

Tissues and Microspheres

Chicken liver and chicken muscle (breast) samples were obtained as fresh samples from the local grocery. Chicken muscle presents a tissue rich in optically birefringent actin-myosin fila-ments. Chicken liver presents a tissue that is cellular in nature with negligible birefringent fibers such as collagen fibers or actin-myosin filaments. Porcine muscle and skin samples were obtained from the local abattoir. The porcine muscle provided a firmer structure than chicken muscle, which allowed very thin sections of muscle to be cut with a razor. The porcine muscle was cut perpendicular to the long axis of the actin-myosin filaments; hence, the filaments were not preferentially oriented along the parallel or perpendicular components of incident polarized light. Chicken muscles appeared to be softer, and the alignment of filaments was easily disordered by compression between glass slides during measurements (see below). This study does not address the issue of how the orientation of muscle
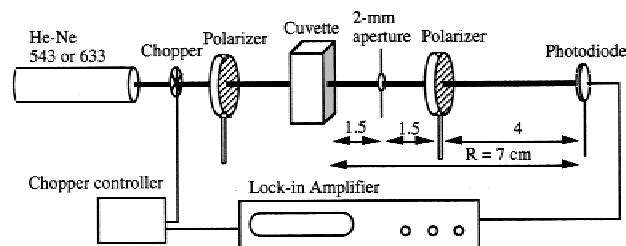
Fig. 3. Experimental setup. The second polarizer between the cuvette and detector selects transmitted light either parallel or perpendicular to the table.

fibers affects polarization measurements, and such studies are in progress by using porcine muscle. Two types of porcine skin samples were obtained, one from an unpigmented domestic pig and one from a strongly melanin-pigmented Yucatan pig.

Polystyrene microspheres were purchased from Tom Pella, Inc. (Redding, CA), Ernest F. Fullam, Inc. (Latham, NY), and Bangs Laboratories, Inc. (Fishers, IN). A range of microsphere diameters (306, 482, 620, 806, 1,069, 2,030, and 6,400 nm) were tested. The refractive index of the spheres at the two visible wavelengths used in these experiments (543 and 633 nm) was 1.59. The microspheres were suspended in aqueous solutions, sometimes with a small amount of alcohol in the solution as shipped from the manufacturer.

Light Scattering Experiment

The experimental apparatus is shown in Figure 3. A helium-neon laser, either a 543-nm or 633-nm wavelength, delivered a 1- to 2-mm diameter beam that was passed through a cuvette holding the sample under test, which was either tissue or a microsphere solution. The transmitted light reach a detector on the rear side of the cuvette. The orientation of the linearly polarized laser beam was aligned horizontal to the table by passing the beam through a horizontally oriented linear polarizer (Ealing Electrooptics, plc., Watford, UK) and rotating the laser to achieve maximal transmission. The cuvette had front and rear plastic windows, and the thickness of the cuvette could be adjusted by moving the front window into different slots of the cuvette assembly. The sides of the cuvette were black. Hence, the pathlength through the cuvette could be adjusted from 0.1 to 1.5 cm. The original concentrated solution of microspheres as delivered from the manufacturer was used. The cuvette pathlength was adjusted to yield a range of optical depths. In the tissue ex-

periments, thin sections of tissue were cut to a desired thickness then sandwiched between the windows of the cuvette with slight pressure to enforce a known thickness. In some cases such as chicken liver and muscle, the tissue thickness could be varied by progressively squeezing the tissue between glass slides. For the pig tissues, which were firmer than chicken tissues, the samples had to be cut to approximately the desired thickness before sandwiching between glass. Some of the microsphere experiments used a standard 1-cm cuvette, and the concentration of microspheres was adjusted to achieve various optical depths. Other microsphere experiments used a variable thickness cuvette and the maximal microsphere concentration obtained from the manufacturer. A 2-mm diameter iris aperture was placed 1.5 cm from the rear of the cuvette to minimize the amount of scattered light that reached the detector. The detector was located 7 cm from the rear of the cuvette and presented a 1-cm diameter collection area. A second polarizer was placed 1.5 cm behind the iris aperture and in front of the detector and was aligned to be parallel or perpendicular to the table, yielding I_{par} and I_{per} measurements. A chopper and lock-in amplifier were used to improve the signal-to-noise of measurements.

Analysis

Consider a beam of linearly polarized light, I_o, incident onto a slab of scattering medium. The incident light is defined as having a parallel orientation. As the photons propagate into the medium, some are scattered and some proceed unscattered to reach the detector located at some distance from the rear surface of the slab. The detector will collect the unscattered component of the incident beam, $I_o\exp(-\mu_sL)$, where μ_s is the scattering coefficient of the medium and L is the thickness of the slab. The detector will also collect a fraction f of the multiply scattered light that transmits through the slab. Hence, the total amount of parallel polarized light will be:

$$I_{par} = I_o\exp(-\mu_sL) + f\,I_{par\ scattered} \qquad (2)$$

and the amount of perpendicularly polarized light will be:

$$I_{per} = f\,I_{per\ scattered}. \qquad (3)$$

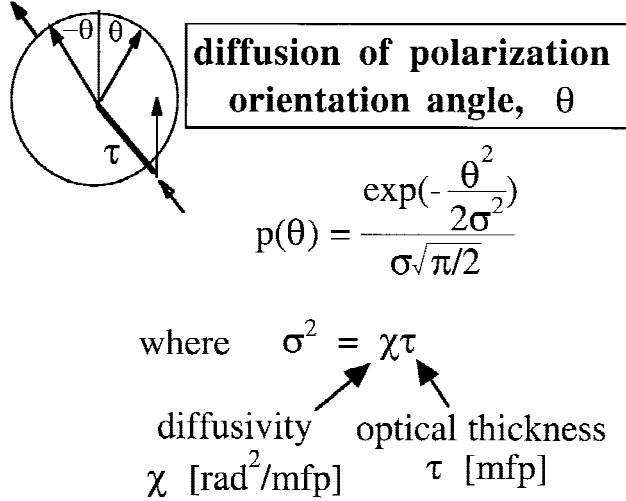We shall be describing experiments in which the optical thickness of the sample, $\tau = \mu_sL$, was

$$p(\theta) = \frac{\exp(-\frac{\theta^2}{2\sigma^2})}{\sigma\sqrt{\pi/2}}$$

where $\sigma^2 = \chi\tau$

diffusivity   optical thickness
χ [rad^2/mfp] τ [mfp]

Fig. 4. Randomization of the orientation of linearly polarized light. As polarized light propagates through an optical depth τ, the angle (θ) of orientation of the linear polarization diffuses in angle space from its original orientation. The rate of diffusion is characterized by the diffusivity χ (rad^2/mean free path).

increased either by varying the concentration of microspheres to alter μ_s or by varying the pathlength L. The transmitted I_{par} and I_{per} were measured as a function of τ.

To estimate the value of scattered light, which is polarized parallel and perpendicular, consider how the orientation of polarization, θ, of scattered photons will diffuse toward larger angles (see Fig. 4). The probability for the orientation of polarized light to be oriented at an angle θ relative to its initial orientation after propagating through some optical thickness τ is postulated in this study to be well approximated by the Gaussian expression:

$$p(\theta) = \frac{\exp\left(-\frac{\theta^2}{2\sigma^2}\right)}{\sigma\sqrt{\pi/2}}, \ \sigma^2 = \chi\tau \quad (4)$$

such that

$$\int_{-\infty}^{\infty} p(\theta) \, d\theta = 1.$$

The value σ is equated to the product of the optical thickness τ (mean free paths or mfp) and a diffusivity χ (radians^2/mfp). The angle θ can diffuse in both the $+\theta$ and $-\theta$ directions relative to the original parallel orientation defined as $\theta = 0°$. Although θ can diffuse beyond an angle of $\pm2\pi$, the factor $p(\theta)$ is Gaussian and continues to drop at large θ.

The amount of parallel light is proportional to the expectation value for $\cos^2(\theta)$, because detected power equals the square of the parallel component of the electric field which is proportional to $\cos(\theta)$. The amount of parallel light is proportional to $\langle\cos^2\theta\rangle$:

$$\langle\cos^2\theta\rangle = \int_{-\infty}^{\infty} p(\theta)\cos^2\theta \, d\theta = \frac{1}{2}\left(1 + \exp\left(-\frac{\sigma^2}{2}\right)\right). \quad (5)$$

Guided by this simple exponential behavior, and substituting $\chi\tau$ for σ^2, the following descriptions for the development of the two factors $I_{par\ scattered}$ and $I_{per\ scattered}$ in Eq. 2 and 3 are postulated:

$$I_{par\ scattered} = I_o(1 - \exp(-\tau)) \, f \exp(-\mu_{atten}L) \frac{1}{2}$$
$$\left(1 + \exp\left(-\frac{\chi\tau}{2}\right)\right) \quad (6)$$

$$I_{per\ scattered} = I_o(1 - \exp(-\tau)) \, f \exp(-\mu_{atten}L) \frac{1}{2}$$
$$\left(1 - \exp\left(-\frac{\chi\tau}{2}\right)\right)$$

where L is the thickness of the sample. The amount of scattered light is $I_o(1 - \exp(-\tau))$. The attenuation of scattered light due to absorption and scattering is approximated by the term $\exp(-\mu_{atten}L)$, which accounts for the slow but steady loss of $I_{par\ scattered}$ and $I_{per\ scattered}$ at larger τ. The term $\exp(-\mu_{atten}L)$ is merely empirically specified from the data of each experiment but is similar to the factor $\exp(-\mu_{eff}L)$ from diffusion theory where μ_{eff} is the effective attenuation coefficient. The μ_{atten} probably includes effects of the cuvette boundaries. The fraction of the scattered light that is parallel polarized is initially 1 and drops to 1/2 as the light becomes randomly polarized. The fraction of scattered light that is perpendicularly polarized is initially 0 and increases to 1/2 as the light becomes randomly polarized (Fig. 5).

Finally, the degree of polarization, Pol, of the collected light is calculated for the I_{par} and I_{per} from equations 2 and 3 after using equation 6:

$$Pol = \frac{I_{par} - I_{per}}{I_{par} - I_{per}}. \quad (7)$$

For small τ, the unscattered light $I_o\exp(-\tau)$ dominates Pol and the value of Pol is 1. Once the contribution of the unscattered primary beam
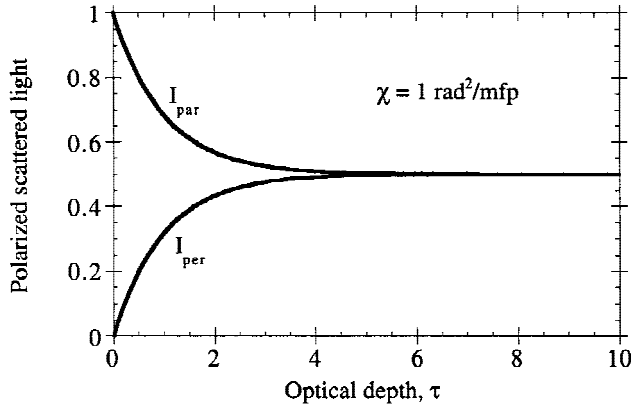
Fig. 5. Transition from parallel polarized to randomly polarized light. The fractions of scattered light which are parallel, $\frac{1}{2}(1 + \exp(-ct/2))$, and perpendicularly oriented, $\frac{1}{2}(1 - \exp(-ct/2))$, are plotted versus the optical depth τ through which the light has propagated. In this example, $\chi = 1$ rad^2/mfp. mfp, mean free path.

drops below the contribution of collected scattered light, the value of Pol becomes dominated by the values of $I_{par\ scattered}$ and $I_{per\ scattered}$. Pol will transition from 1 to 0 at a rate which is determined by the diffusivity χ.

Figure 6 illustrates the behavior of typical experimental data for a range of possible χ values from 0 to 0.5 in steps of 0.05 rad^2/mfp. In the top figure, the measured signals I_{par}/I_o and I_{per}/I_o (dimensionless) are plotted on the y-axis. The x-axis is the optical thickness, $\tau = \mu_s L$, in the dimensionless units of mfp. The source I_o was parallel polarized. In the lower figure, the polarization fraction Pol falls from 1 to 0 at different rates depending on the choice of the diffusivity χ. χ is the apparent diffusivity (rad^2/mfp) for the angle of orientation of linearly polarized light per unit pathlength of optical thickness. A family of curves for various $\chi = 0$–0.5 in steps of 0.05 is shown, with larger χ values causing more rapid transition of Pol from 1 to 0. During curve fitting, the initial slope of I_{par}/I_o specifies μ_s, the final slope at large τ midway between the I_{par}/I_o and I_{per}/I_o curves specifies μ_{atten}. The y-offset of this final slope at large τ and how closely I_{par}/I_o and I_{per}/I_o approach each other at large τ are the two factors that specify f and χ. In Figure 6, the example assumed $f = 1 \times 10^{-4}$, $\mu_{atten} = 8$ cm^{-1}, $\mu_s = 40$ cm^{-1} and L was varied from 0 to 1 cm to achieve various τ values.

Influence of f

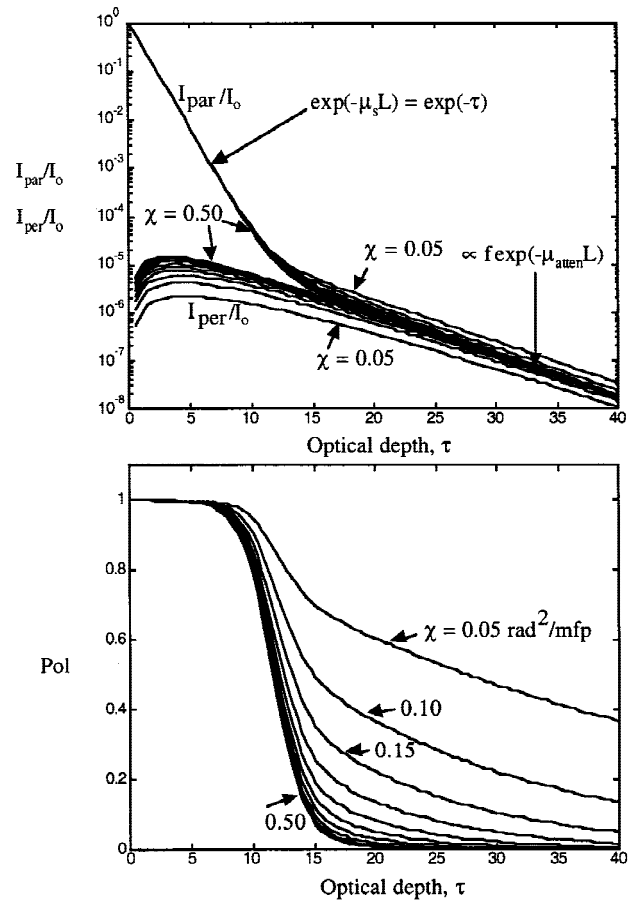The fraction f of scattered light collected by the detector depends on several factors. The value

Fig. 6. Example of simulated typical data. The family of curves are for a series of choices of χ ranging from 0 to 0.5 in steps of 0.05 rad^2/mfp. (Top) The parallel and perpendicular components of transmitted light, I_{par}/I_o and I_{per}/I_o, are plotted versus the optical depth τ. The initial attenuation of incident parallel polarized light falls as $\exp(-\tau)$. Once the incident beam is attenuated, the scattered light dominates the measurement and falls as $\exp(-\mu_{atten}L)$. The factor f specifies when scattered light begins to dominate. The curves are only modestly affected by χ. (Bottom) The polarization factor, pol, is plotted versus τ. Once the scattered light begins to dominate the measurement, pol drops from 1 to 0 at a rate that is strongly dependent on χ.

f depends on the solid angle of collection presented by the 1-cm-diameter photodiode detector placed at a cuvette-detector distance R equal to 7 cm. If the detector is placed at larger R, then the 2-mm-diameter aperture located 1.5 cm from the cuvette rear surface would begin to restrict the solid angle of collection. The value of f is also influenced by the optical depth τ of the sample in the cuvette. For low optical depths caused by low concentrations of microspheres or thin sections of tissue or microsphere solution, the scattered light would still be rather forward directed and the value of f would be higher. For larger optical

depths caused by high microsphere concentrations or thick samples, the value of f would drop to a low value typically in the range of 10^{-4}. We used Monte Carlo simulations and experiments to study how various factors affected f and how such a variable f would affect the fitting of experimental data as described above. The results (not shown here) demonstrated that f was principally influenced by the solid angle of collection by the detector. The dependence of f on τ at lower τ values was found to have only a small effect on the fitting of experimental data. Hence, in this study, a constant f value was used during the fitting of each experiment data set (I_{par}/I_o and I_{per}/I_o versus a range of τ values). The errors in the reported χ values caused by ignoring the variable nature of f are less than the variation in reproducibility of experimental measurements.

RESULTS

Figures 7 and 8 show some typical examples of experimental data at 633 nm. The two examples are a polystyrene microsphere solution in Figure 7 and chicken liver in Figure 8. The microspheres had a diameter of 0.482 μm and were at a concentration of 0.0026% volume fraction or C = 4.52×10^8 cm^{-3}, which yielded a scattering coefficient of μ_s = 8.0 cm^{-1}. Fitting the data, the values f = 30×10^{-4}, μ_{atten} = 1.5 cm^{-1} and χ = 0.070 rad^2/mfp were obtained. For the chicken liver sample, the scattering coefficient was estimated from the values of reported μ_s values for liver in the table of optical properties compiled by Cheong et al. [17] to be about μ_s = 290 cm^{-1} at 633-nm wavelength. Fitting the data, the values f = 0.65 $\times 10^{-4}$, μ_{atten} = 0.45 cm^{-1} and χ = 0.00070 rad^2/mfp were obtained. Other microsphere solutions and tissue samples showed similar behavior.

Table 1 and Figure 9 show a summary of the χ values obtained from the analyses, based on the mean of typically three samples with standard deviations in the range of 10–50% of the mean. On the left, the x-axis is the microsphere diameter (μm) and the y axis is the χ value (rad^2/mfp). On the right, the χ values for tissues are plotted in order of increasing χ value. The results show data at both the 543 and 633 nm wavelengths. Figure 9 also shows the χ values derived from the experimental data of Jarry et al. [16] for microspheres and calf liver. The analysis for their calf liver assumed the same scattering as above, μ_s = 290 cm^{-1}. The domestic and Yucatan pig skin samples yielded nearly identical χ values, so the melanin
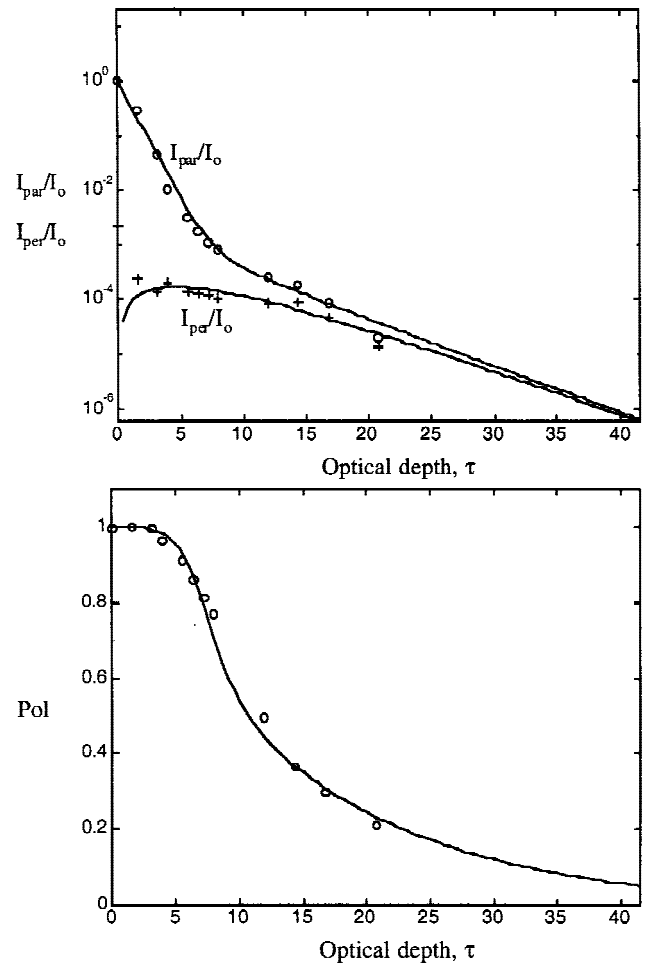

Fig. 7. Experimental data for polystyrene microspheres, 482-nm diameter.

content did not affect the measurement. The value of χ varied in the order liver < muscle < skin.

A more strictly appropriate graph, from the perspective of Mie scattering theory, would plot the x-axis of Figure 9 as the size factor, $\times$ = π(dia)/(λ/n$_{water}$), which is dimensionless and accounts for the wavelength dependence of Mie scattering from the microspheres. Such a plot was created (not shown) but did not improve the behavior of the data. The experimental variation of χ was greater than the wavelength dependency of $\times$ for the two wavelengths.

DISCUSSION

This work suggests that the randomization of linear polarization during transmission through a tissue is more rapid in birefringent tissues than in nonbirefringent tissues. The most
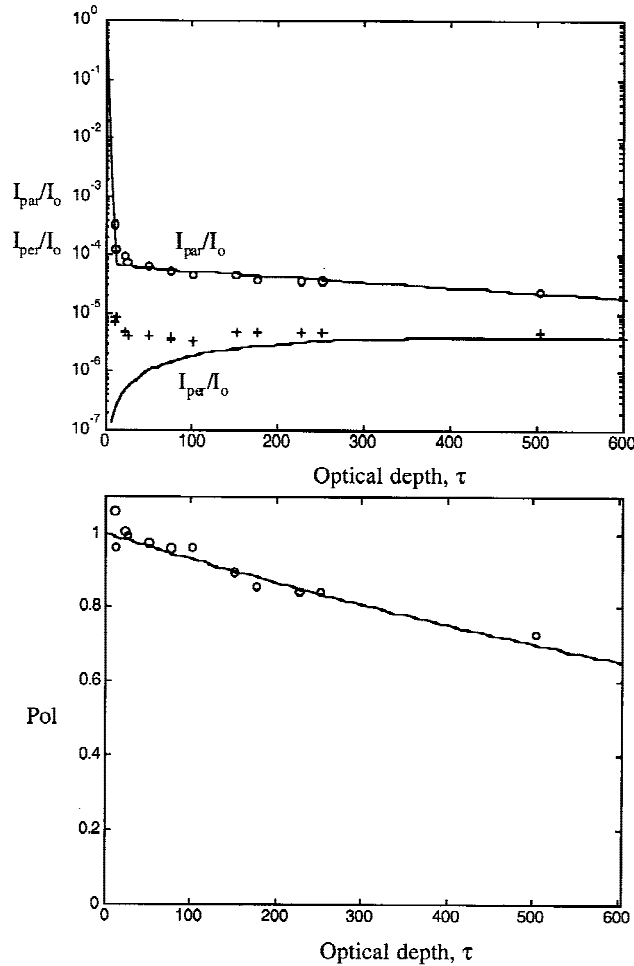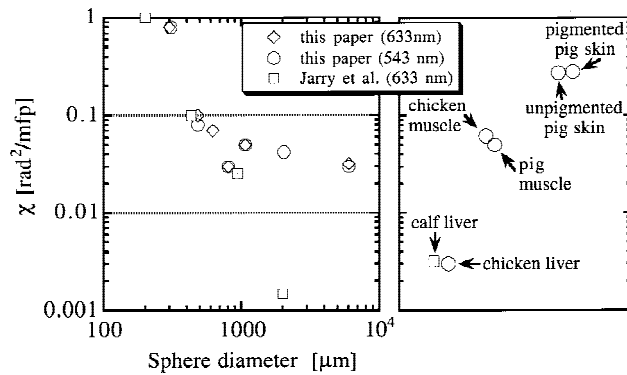
Fig. 8. Experimental data for chicken liver.

Fig. 9. Summary of diffusivity χ [rad^2/mfp] of polystyrene microspheres and various ex vivo tissues. (Left) Diffusivity plotted versus microsphere diameter. (Right) Tissue diffusivity. Data from this study are represented as circles and diamonds. Data from Jarry et al. [17] are represented as squares.

rapid depolarization occurred in skin and the slowest depolarization occurred in chicken liver. Muscle showed an intermediate rate of depolarization. Recall that muscle is loaded with birefrin-

TABLE 1. Experimental Values for Scattering Coefficient and Angular Diffusivity of Linearly Polarized Light

Microsphere diameter (μm)	Scattering coefficient μ_s (cm^{-1})	Angular diffusivity χ (rad^2/mfp)	Wavelength (nm)
300	9.1	0.80	633
482	5.3	0.10	633
620	6.6	0.070	633
806	6.4	0.030	633
1070	23	0.050	633
2030	7.0	0.032	633
308	5.2	0.80	543
482	5.0	0.080	543
806	6.35	0.030	543
1070	1.11	0.050	543
2030	6.3	0.042	543
6040	2.7	0.030	543
Tissues:			
Chicken liver	290	0.0004	633
Chicken muscle	250	0.60	633
Pig muscle	210	0.055	543
Domestic pig skin	187	0.273	543
Yucatan pig skin	187	0.280	543

gent actin-myosin filaments and dermis is loaded with birefringent collagen fibers. Chicken liver is a jelly-like cellular mass with negligible collagen fibers and is nonbirefringent.

The speed of polarized light whose electric field is oriented along the fibers is different than the speed of polarized light whose electric field is oriented perpendicular to the fibers. When linearly polarized light propagates at odd angles to birefringent fibers the parallel and perpendicular components of the light, relative to the fiber axis, will become out of phase and the angular orientation of the net linear polarization will rotate. If the tissue fibers are perfectly aligned, the orientation of linear polarization will simply rotate, just as would occur in an ideal optical retarder. If the tissue fibers are not near perfectly aligned, the orientation of linear polarization for different photons will rotate at different rates and the linearly polarized light will randomize. For example, dermal collagen fibers are somewhat randomly oriented with respect to angle although they are oriented roughly horizontally in the horizontal plane of the skin. Hence, linearly polarized incident on the skin will be rapidly depolarized by dermal collagen. The literature on birefringence of tissues is large and further reading may begin with Maitland and Walsh [18] and Sankaran and Walsh [19].

The angular diffusivity χ described in this study is convenient and descriptive, but has limits. If birefringent fibers are well aligned, then the

polarization will rotate in one specific angular direction rather than diffusing equally in both directions as assumed by our diffusion analysis. We are currently exploring the effects of alignment of actin-myosin fibers in pig skeletal muscles on the rotation and randomization of polarized light. For this study, we oriented our pig skeletal fibers axially such that light traveled along the fiber axis and both parallel and perpendicular components of the electric field were oriented perpendicular to the fiber, thereby avoiding the issue of fiber alignment. The chicken muscle was quite soft and its fiber alignment was easily disorganized by compression between glass slides.

The polystyrene microspheres present spherical surfaces of refractive index discontinuity that scatter polarized light into new directions. After incident parallel polarized light is scattered, the parallel and perpendicular components of the polarized light yield a new net orientation of linear polarization. Consequently, each scattering event by microspheres alters the orientation of linear polarization. This mechanism of reorienting polarized light after each scattering by a microsphere is fundamentally different than the mechanism of depolarization due to randomly oriented birefringent fibers in biological tissues, even though the result is similar.

The results suggest an estimate of the depth of imaging achieved by the polarized light camera. The epidermis and initial papillary dermis apparently allow penetration of linearly polarized light with modest depolarization. The camera images are based on backscattered polarized light during the initial penetration of polarized light through the epidermis and initial papillary dermis. However, the dermal collagen fibers rapidly depolarize the incident light. The angular diffusivity χ for skin reported in this study is about 0.28 rad^2/mfp which will cause the polarization (Pol) to drop from unity to nearly zero after 10 mfp. Because polarized photons must both enter and exit the dermis, the depth of dermis that would contribute to a polarization image would be 5 mfp. The scattering coefficient μ_s is 187 cm^{-1} and the mfp equals $1/\mu_s = 1/187 = 53$ μm. Therefore, the depth of polarization imaging is expected to about 5 (53 μm) or 265 μm beyond the epidermis, which is typically about 60–100 μm in thickness. The polarization images would strongly depend on scattering from epidermal structures and on scattering from dermal structures with decreasing weight as a function of depth into the dermis down to a maximal depth of 326–367 μm from the tissue surface. In summary, polarization should image the upper few hundred micrometers of skin, including the superficial layer of the dermis. Hence, images should be sensitive to any disruption of the dermis by skin cancer invading from the epidermis.

REFERENCES

1. Jacques SL, Lee K, Polarized video imaging of skin. SPIE Proceedings 3245D, Cutaneous Applications of Lasers: Dermatology, Plastic Surgery, and Tissue Welding, San Jose, CA. February 26–28, 1998.
2. Torrance KE, Sparrow EM, Birkebak RC. Polarization, direction distribution, and off-specular peak phenomena in light reflected from roughened surfaces. J Opt Soc Am 1966;56:916–925.
3. Wolff LB, Polarization camera for computer vision with a beam splitter. JOSA-A 1994;11:2935–2945.
4. Jones BF, Fairney PT. Recognition of shiny dielectric objects by analyzing the polarization of reflected light. Image and Vision Computing 1989;7:253–258.
5. Bickel WS, Davidson JF, Huffman DR, Kilkson R. Application of polarization effects in light scattering: a new biophysical tool. Proc Natl Acad Sci USA 1976;73:486–490.
6. Anderson RR. Polarized-light examination and photography of the skin. Arch Dermatol 1991;127:1000–1005.
7. Schmitt JM, Gandjbakhche AH, Bonner RF. Use of polarized light to discriminate short-path photons in a multiply scattering medium. Appl Optics 1992;32:6535–6546.
8. Dogariu M, Asakura T. Photon pathlength distribution from polarized backscattering in random media. Opt Eng 1996;35:2234–2239.
9. Jacques SL, Wang LH, Stephens DV, Ostermeyer M. Polarized light transmission through skin using video reflectometry: toward optical tomography of superficial tissue layers. In: Anderson RR, editor. Lasers in surgery: advanced characterization, therapeutics, and systems VI. Proc SPIE 1996;2671:199–220.
10. Ostermeyer MR, Stephens DV, Wang L, Jacques SL. Nearfield polarization effects on light propagation in random media. In: Sevick-Muraca E, Benaron D, editors. OSA TOPS on biomedical optical spectroscopy and diagnostics, vol 3. Washington, DC: Optical Society of America; 1996. p 20–25.
11. Hielscher AH, Mourant JR, Bigio IJ. Influence of particle size and concentration on the diffuse backscattering of polarized light from tissue phantoms and biological cell suspensions. Appl Optics 1997;36:125–135.
12. Demos SG, Alfano R.R. Optical polarization imaging. Appl Optics 1997;36:150–155.
13. Hielscher AJ, Eick AA, Mourant JR, Shen D, Freyer JP, Bigio IJ. Diffuse backscattering Mueller matrices of highly scattering media. Optics Express 1997;1:441–453.
14. Cameron B, Coté G, Rakovic M, Kattawar G, Mehrubeoglu M, Rastegar S, Wang HV. Diffusely backscattered polarized light Mueller matrix imaging of a turbid media. Spring Topical Meetings, Optical Society of America, Orlando, FL, March 8–11, 1998.
15. Mourant JR, Hielscher AH, Freyer JP, Johnsom TM,

Eick AA. Scattering properties of biological cells. Spring Topical Meetings, Optical Society of America, Orlando, FL, March 8–11, 1998.

16. Jarry G, Steimer E, Damaschini V, Epifanie M, Jurczak M, Kaiser R. Coherence and polarization of light propagating through scattering media and biological tissues. Appl Optics 1998;37:7357–7367.

17. WF Cheong. Appendix to Chapter 8: Summary of Optical Properties. In: Welch AJ, van Gemert MJC, editors. Optical-thermal response of laser-irradiated tissue. New York: Plenum Press; 1995.

18. Maitland DJ, Walsh JT Jr. Quantitative measurements of linear birefringence during heating of native collagen. Lasers Surg Med 1997;30:310–318.

19. Sankaran V, Walsh JT Jr. Birefringence measurement of rapid structural changes during collagen denaturation. Photochem Photobiol 1998;8:846–851.